www.ijprems.com
editor@ijprems.com

INTERNATIONAL JOURNAL OF PROGRESSIVE RESEARCH IN ENGINEERING MANAGEMENT AND SCIENCE (IJPREMS)
(Int Peer Reviewed Journal)
Vol. 04, Issue 12, December 2024, pp : 844-852

e-ISSN : 2583-1062
Impact Factor : 7.001

DESIGN AND SIMULATION OF HIGH GAIN ISOLATED DAB BI-DIRECTIONAL DC-DC CONVERTER FOR EV APPLICATIONS

T. Dhananandhan[1], V. Geetha[2]

[1]PG Scholar, Power Electronics and Drives, Government college of Engineering salem, India.

[2]Professor and Head of the Department EEE, Government college of Engineering, Salem-636 011, Tamil Nadu, India.

ABSTRACT

This design provides an overview on the implementation of a Dual Active Bridge (DAB) DC/DC converter. To analyse and find the problem of existing converter topology. This can be modify and design the converter topology to achieve the high gain that significantly increase the voltage from the input to the output side. Ensuring electrical isolation between input and output to enhance safety. It develop Bi-Directional topology, allowing energy to flow both ways, which is crucial for charging EVs and feeding energy back to the grid. DAB topology offers advantages like soft-switching commutations, a decreased number of devices and high efficiency. The design is beneficial where power density, cost, weight, galvanic isolation, high-voltage conversion ratio, and reliability are critical factors, making this design an excellent choice for EV charging stations and energy storage applications. Modularity and symmetrical structure in the DAB allow for stacking converters to achieve high power throughput and facilitate a bidirectional mode of operation to support battery charging and discharging applications. simulate the designed converter topology and obtain the expected results.

Key words- Bidirectional; DC–DC converter; Dual Active Bridge(DAB); Isolation; High Gain; EV application

1. INTRODUCTION

The electric vehicle charging standards governed by the Combined Charging System and CHAdeMO® are constantly changing and are pushing for faster battery charging rates requiring typically less than 30 minutes spent at a charging station for one full charge of an electric vehicle. The DC charging station is typically a Level 3 charger which can cater to a very high power level between 120–240 kW. These DC charging stations are standalone units which house AC/DC and DC/DC power conversion stages. A number of power conversion modules are stacked together inside of a charging station to increase the power levels and enable fast charging. DC fast-charging stations provide a high power DC current to an electric vehicle's battery without passing through any onboard AC/DC converter, which means the current is connected directly to the battery. Most cars on the road today can handle only up to 50 kW. Newer cars have the ability to charge at greater rates of power.

The DC/DC converter in a charging station must be capable of interfacing with the rectified bus voltage (700–800 V) from a three-phase Vienna rectifier at the input and connect with the battery of an electric vehicle at the output, delivering rated power. The DC/DC converter finds important application in a number of end equipment. As EVs come with higher range and batteries get bigger, DC charging solutions are being developed to support long-range EV batteries through fast charging stations up to 250 kW or more.

The DC/DC converter must be capable of handling high power levels. In addition to this, the converter must be modular, which enables single power stage converter units to be paralleled, whereby the output power throughput can be scaled to higher levels as required by DC charging station standards. Current trends in the charging station are moving toward converters that can handle bidirectional power flow. New practices, such as Vehicle-to-Grid (V2G), involve power transfer between the battery of an electric vehicle and the AC grid. Bidirectional DC/DC converters enable charging of the battery in the forward mode of operation and facilitate flow of power back to the grid from the battery during reverse mode of operation, which can be used to stabilize the grid during peak load periods.

Power density and system efficiency are two important requirements of a converter in a DC charging station. Operating at high switching frequencies enables reduced size of magnetics. By moving to higher bus voltage to facilitate fast charging, more power can be transferred at the same current level. This helps to reduce the amount of copper, thereby improving power density of the converter. The converter must also be highly efficient as it results in significant cost savings and reduced thermal solution. This reduced thermal solution directly translates into reduced and compact heat sink size, which in turn increases the power density of the converter. The converter must also be capable of inherent soft switching like ZVS (Zero Voltage Switching) and ZCS (Zero Current Switching) without the addition any bulky passive components which might hamper power density.

The DC/DC converter must be capable of interfacing seamlessly with Lithium ion or a lead acid battery, which are predominantly used in EV charging stations. The DC/DC converter must also be capable of providing the required voltage conversion between the high-voltage and low-voltage side and provide galvanic isolation between them.

www.ijprems.com
editor@ijprems.com
INTERNATIONAL JOURNAL OF PROGRESSIVE RESEARCH IN ENGINEERING MANAGEMENT AND SCIENCE (IJPREMS)
(Int Peer Reviewed Journal)
Vol. 04, Issue 12, December 2024, pp : 844-852
e-ISSN : 2583-1062
Impact Factor : 7.001

In this simulation, closed-loop control for both directions of power flow is simulated using PI controller, which is placed on the LV side. The transition to digital power control indicates that functions are now implemented in software. In addition to the flexibility, this capability adds to and simplifies the system. These systems can implement advanced control strategies to optimally control the power stage under different conditions and also provide system level intelligence to make safe and seamless transitions between operation modes and pulse width modulated (PWM) switching patterns.

2. PROPOSED SYSTEM

2.1 CIRCUIT OF PROPOSED SYSTEM

Power transfer happens in a dual-active bridge where two high-frequency square waves are created in the primary and secondary side of the transformer by the switching action of MOSFETs. Power transfer takes place from the leading bridge to the lagging bridge, and this power flow direction can be easily changed by reversing the phase shift between the two bridges.

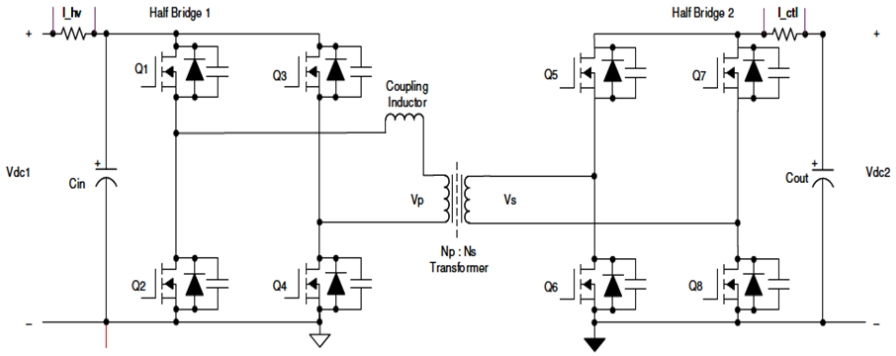

Figure 2.1 Circuit Diagram Of Proposed System

In this figure 2.1 shown the diagram of proposed system that that the Isolated Dual Active Bridge (DAB) Bidirectional DC-DC Converter offers several solutions that make it highly suitable for applications like electric vehicle (EV) charging and micro grids.

2.2 DESIGN OF CONVERTER AND OPERATING PRINCIPLES

The primary specifications for designing a power converter system are input voltage V1, output voltage V2, and the maximum required power transfer. The power transfer relation of the dual-active bridge is given by Equation 1. The best value for N is V_1,nom / V_2,nom, which is 1.6 for this designs specifications.

$$P = \frac{N\ V\_1\ V\_2\ \varphi\ (\pi - |\varphi|)}{(2\pi\neg 2FsL)} \quad (1)$$

The phase shift of the converter is dependent on the value leakage inductor. The phase shift for required power transfer is given by Equation 3.3.

$$\varphi = \pi/2\ \times 1 - \sqrt{(1 - (8 \times Fs \times L \times P\_out)/(N \times V\_1 \times V\_2))} \quad (2)$$

Required phase shift in degrees over leakage inductance for V1 = 800 V, V2 = 500 V, N = 1.6, Fs= 100 kHz, and Pout= 10 kW. The graph illustrates that for a small value of inductance, a maximum power transfer at a small value of phase shift is obtained. To have fine control over power transferred, fine high-resolution steps in which the phase can be varied must be obtained. Alternatively, a larger inductor can obtain maximum power transfer at a high value of phase shift for better control. For the selected L = 35 µH, a phase shift of 23 degrees or 0.4 radians is required.

DC Blocking capacitors are introduced in the power stage to avoid saturation of the transformer in case of unbalanced currents, which can be caused by mismatched PWM signals, mismatched propagation delays in gate drivers or other asymmetries in the system. Especially during start-up and load transients unbalanced currents can occur. The DC blocking capacitors must be designed to handle the RMS currents on the transformer, be able to withstand the full-voltage and provide enough capacitance to not influence the switch node voltage waveforms in a significant manner.

$$C_{DcBlock} = \frac{100}{(4\times\pi 2\times F2\times L)} = 7.2\mu F \quad (3)$$

2.2.1 CALCULATION OF INDUCTOR AND CAPACITOR OF CONVERTER

The output capacitor in the dual-active bridge must be designed to handle the ripple. The capacitor current is the difference between the current IHB2 and the output current ILoad, also called Iout. The best output current Iout is obtained by Pout / V2. From the difference between Iout and IHB2 the charge ΔQ can be obtained. Afterwards, the required capacitance can be calculated using Equation (5) for a maximum allowed ripple voltage. This results in ΔQ of

www.ijprems.com
editor@ijprems.com
INTERNATIONAL JOURNAL OF PROGRESSIVE RESEARCH IN ENGINEERING MANAGEMENT AND SCIENCE (IJPREMS)
(Int Peer Reviewed Journal)
Vol. 04, Issue 12, December 2024, pp : 844-852
e-ISSN : 2583-1062
Impact Factor : 7.001

12μC for 10-kW output power and nominal input and output voltages. For lower output voltages, ΔQ increases to 50μC. Using Equation (5) and a voltage ripple of 5 V leads to a required output capacitance of 10μF. Therefore 470μF of output capacitance is necessary to reduce the ripple to 5%.

$$C_{out} = \frac{\Delta Q}{V_{ripple}} = 470\ \mu F \qquad (4)$$

Equation (1) shows that the power transfer can be controlled with the phase shift φ, where the maximum power transfer occurs for $\varphi = \pi / 2$. With V_1 and V_2 fixed, there are two variables left to design for the required output power. These are the switching frequency Fs and the leakage inductance L. With Fs set to 100 kHz, L is selected as 35 μH. This leaves some headroom above the target power of 10 kW, which is required for lower output voltages.

$$L = \frac{(N\ V\_1\ V\_2\ \varphi\ (\pi - |\varphi|)}{(2\pi^2 FsP)} = 35\mu H \qquad (5)$$

2.2.2 MODE OF OPERATION

During interval one, the inductor current waveform is both positive and negative, and hence, the current commutation follows the scheme below. During this interval, switches Q1 and Q4 in the primary and switches Q6 and Q7 in the secondary conduct current. During this interval, the voltage across the primary, Vp, is equal to V1, and the voltage across the secondary, Vs, is equal to V2. The difference between these voltages appears across the leakage inductor, and the slope of the current during this interval can be approximated $\frac{di}{dt} = \frac{V1+V2}{L}$

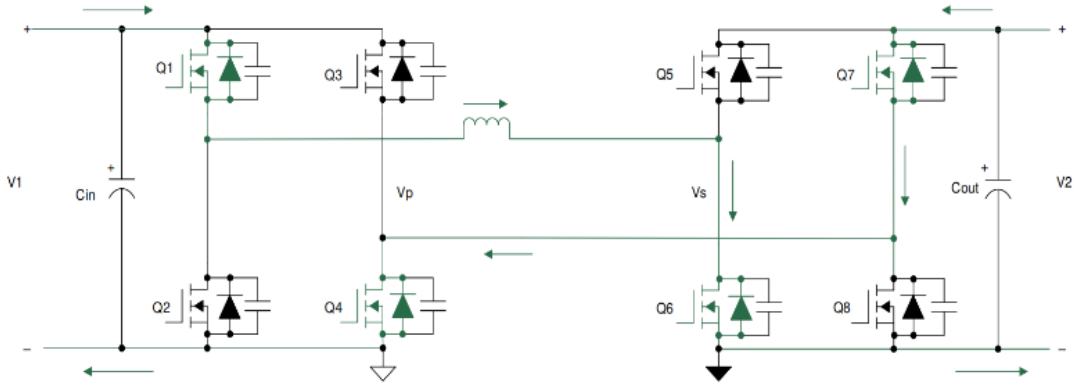

Fig.2.2 Interval-1

During interval two, the inductor current is positive. The voltage across the transformer primary is positive and is equal to V1, and the voltage across the secondary winding is positive and is equal to V2. Hence, the difference of these two voltages appears across the leakage inductor, and the slope of the rising current during this interval can be calculated by equation. $\frac{di}{dt} = \frac{V1-V2}{L}$ During this interval, switches Q1 and Q4 remain turned on, but as the voltage across the secondary is now V2 with the inductor current positive, switches Q5 and Q8 turn on to conduct current. There is a small dead time period between the turn off of Q6 and Q7 and the turn on of Q5 and Q8. During this dead time, the phenomenon of zero voltage switching (ZVS) occurs. The commutation sequence for the second interval is shown below.

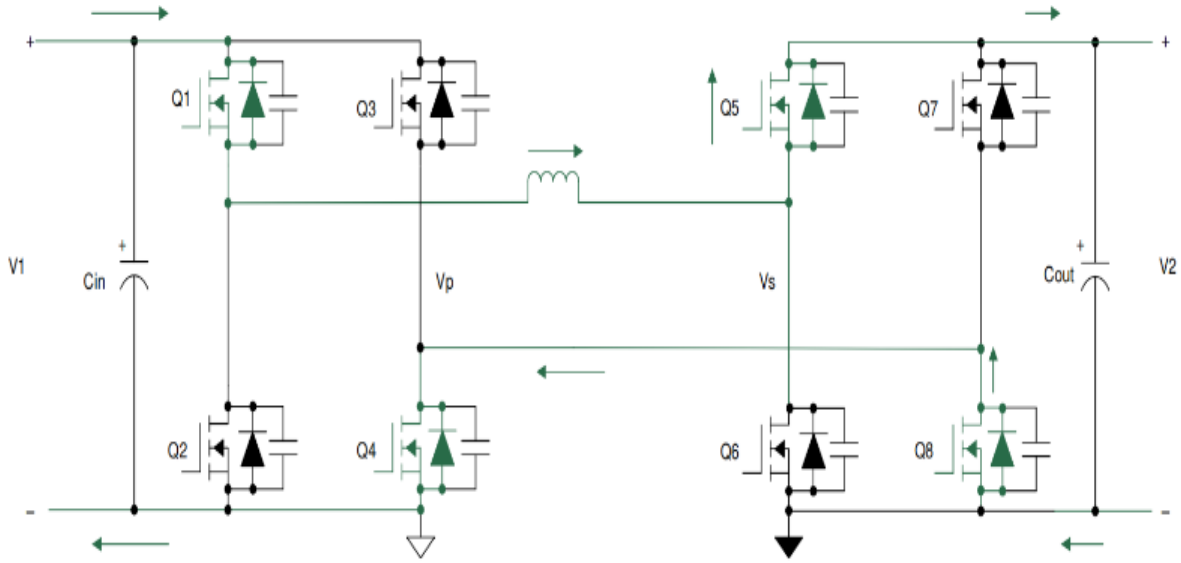

Fig.2.3 Interval-2

www.ijprems.com
editor@ijprems.com
INTERNATIONAL JOURNAL OF PROGRESSIVE RESEARCH IN ENGINEERING MANAGEMENT AND SCIENCE (IJPREMS)
(Int Peer Reviewed Journal)
Vol. 04, Issue 12, December 2024, pp : 844-852
e-ISSN : 2583-1062
Impact Factor : 7.001

During interval three, the inductor current starts ramping down from the positive peak to a negative value. In this interval, the voltage across the primary is –V1, and the voltage across the secondary is V2. The difference of these voltages, which is (-V1-V2), appears across the inductor. Hence, the current ramps down with a negative slope as shown in equation. $\frac{di}{dt} = -\frac{V1+V2}{L}$

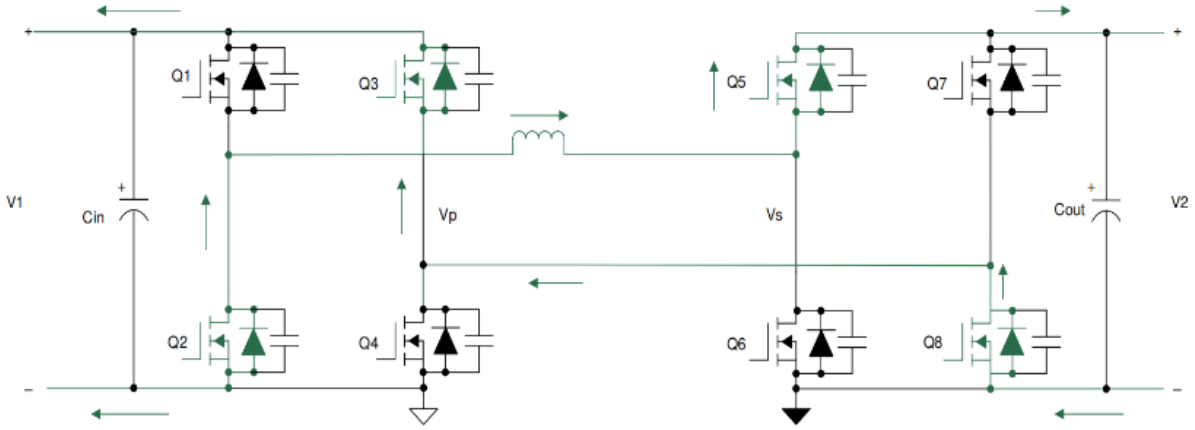

Fig2.3;mode off circuit diagram

During interval four, the inductor current continues to be negative. During this interval, the voltage across the primary is –V1 and, and the voltage across the secondary is -V2.

The difference in these voltages, which is (-V1+V2), appears across the inductor. Hence, the current ramps down with a negative slope as shown in equation. During this interval, switches Q2 and Q3 continue to remain turned on, but as the voltage across the secondary are now –V2, switches Q6 and Q7 turn on to conduct current as shown below.

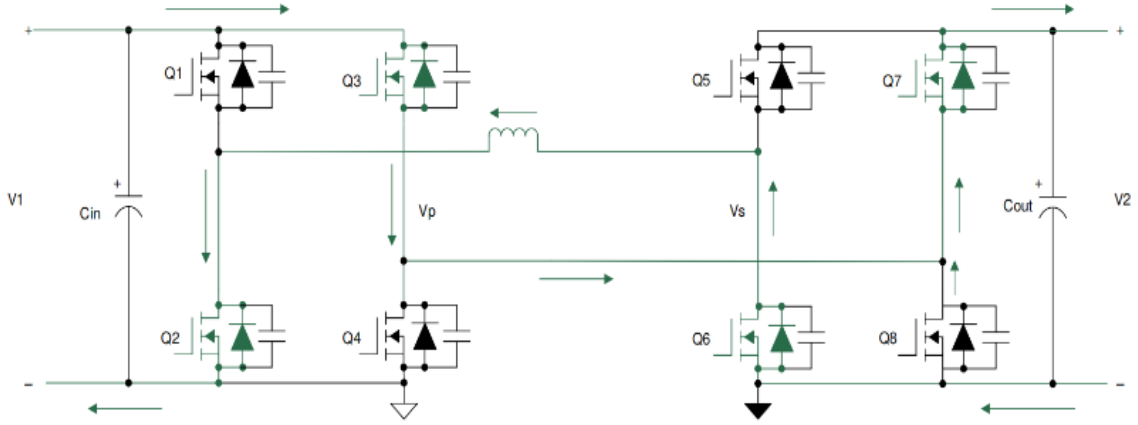

Fig.2.4 Interval-3

2.2.2 DUAL ACTIVE BRIDGE – ZERO VOLTAGE SWITCHING (ZVS)

Between turn-off of one MOSFET and turn-on of the other MOSFET of a branch there is dead time. During this dead time the energy stored in the inductor discharges the output capacitances of the MOSFETs and holds them close to zero voltage before they are turned on. This phenomenon, where the voltage across the MOSFET is close to zero at turn on, is referred to as zero voltage switching (ZVS).

This is a major advantage with this topology, where due to the natural lagging current in one of the bridges, the inductive stored energy causes ZVS of all of the lagging bridge switches and some of the switches of the leading bridge. This depends on the stored inductive energy (EL = 0.5LI2) available to charge and discharge the output capacitances of MOSFETs (EC = 0.5CV2), which again depends on the load of the converter and the input to output voltage ratio. Here the principal of ZVS is explained with the transition from interval one to interval two. Similar analysis can be done for all turn-on events. for all turn-on events.

When transition happens from interval one to two, the primary side switches Q1 and Q5 continue conduction, whereas in the secondary, Q6 and Q7 turn off and Q5 and Q8 turn on. Initially the voltage across Q6 and Q7 is zero when conducting, and Q5 and Q8 block the entire secondary voltage.

During dead time, when all of the switches in the secondary are off, the inductor-stored energy circulates current which discharges the capacitor across MOSFETs Q5 and Q8 to zero and charges the capacitor across MOSFETs Q6 and Q7 to the full secondary voltage. The current commutation is shown below.

www.ijprems.com
editor@ijprems.com
INTERNATIONAL JOURNAL OF PROGRESSIVE RESEARCH IN ENGINEERING MANAGEMENT AND SCIENCE (IJPREMS)
(Int Peer Reviewed Journal)
Vol. 04, Issue 12, December 2024, pp : 844-852
e-ISSN : 2583-1062
Impact Factor : 7.001

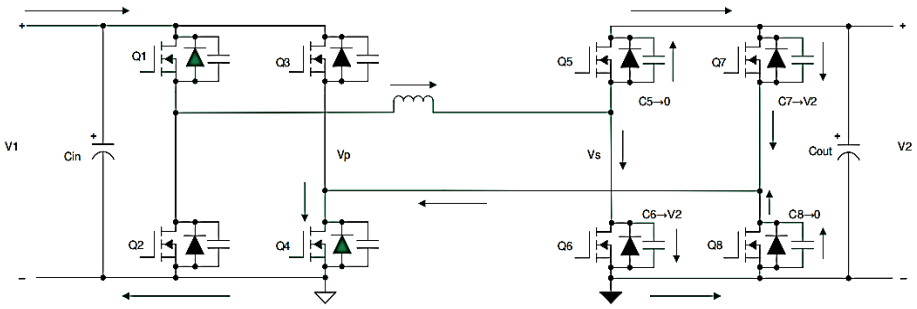

ZVS Transition in Secondary Side – Capacitor

Once the capacitors have been charged and discharged, the current must continue to flow. The current flows through the diodes D5 and D8, thereby clamping the voltage across MOSFETs Q5 and Q8 to zero as shown below. During the next interval, MOSFETs Q5 and Q8 are turned on at zero voltage, thereby reducing turn on losses completely. The arrow close to the diode indicates that the diode is conducting and the MOSFET is off.

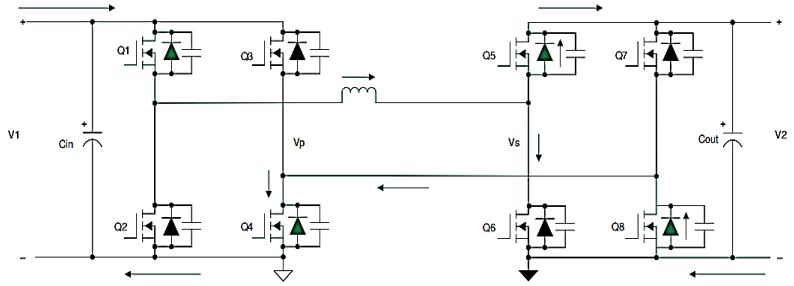

ZVS Transition in Secondary Side – Diode

Similarly, zero voltage switching across the switches of the primary during the transition from interval 2 to 3 is explained in the following section. When transition happens from interval two to three, the secondary side switches Q5 and Q8 continue conduction, whereas in the primary, Q1 and Q4 turn off and Q2 and Q3 turn on. Initially, the voltage across Q1 and Q4 is zero when conducting, and Q2 and Q3 block the entire secondary voltage. During dead time when all of the switches in the primary are off, the inductor stored energy circulates current, which discharges the capacitor across MOSFETs Q2 and Q3 to zero and charges the capacitor across MOSFETs Q1 and Q4 to the full primary voltage. The current commutation is shown below.

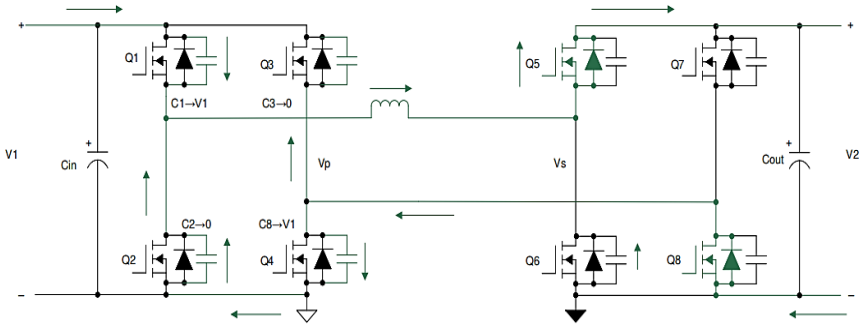

ZVS Transition in Primary Side – Capacitor

Once the capacitors have been charged and discharged, the current must continue to flow. The current flows through the diodes D5 and D8, thereby clamping the voltage across MOSFETs Q5 and Q8 to zero as below. During the next interval, MOSFETs Q5 and Q8 are turned on at zero voltage, thereby reducing turn on losses completely. The arrow close to the diode indicates that the diode is conducting and the MOSFET is off.

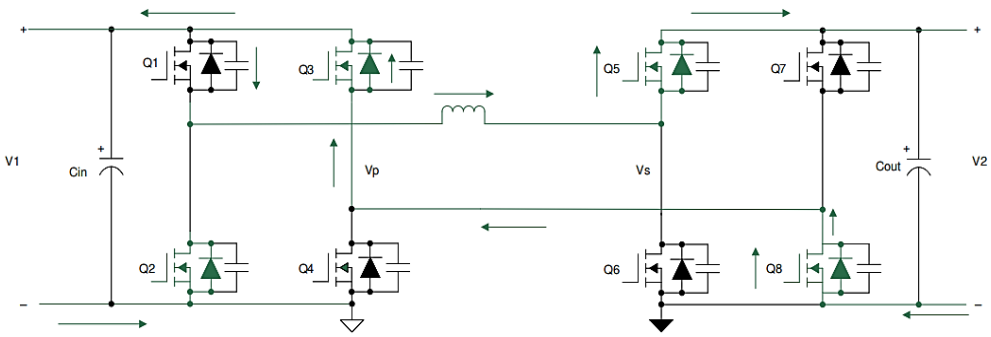

www.ijprems.com
editor@ijprems.com

INTERNATIONAL JOURNAL OF PROGRESSIVE RESEARCH IN ENGINEERING MANAGEMENT AND SCIENCE (IJPREMS)
(Int Peer Reviewed Journal)
Vol. 04, Issue 12, December 2024, pp : 844-852

e-ISSN : 2583-1062
Impact Factor : 7.001

2.4.2 PI CONTROLLER

The PI Proportional and Integral controller is a widely utilized technique in control systems to rectify the discrepancy between the desired setpoint and the actual value, based on feedback. Over the past decade, Permanent Magnet Brushless DC (BLDC) motors have found significant applications in various industries such as E-mobility (Electric vehicles, Electric bicycles), Industrial robots, and CNC machine tools. BLDC motors are crucial components in numerous industrial automation applications due to their exceptional efficiency and high torque-to-power ratios. Unlike traditional motors, Brushless DC motors operate without brushes on the rotor, resulting in minimal maintenance requirements. In the presented approach, the Hall Effect sensors are employed to commutate the BLDC motor. Furthermore, an algorithm is proposed for closed-loop PWM speed control of BLDC motors, where a predetermined value or user control is utilized to regulate the motor speed.

Table 1- PI Controller block properties

PARAMETER	SYMBOL	VALUE
Proportional gain	k_p	0.15
Integral gain	k_i	15

3. SIMULATION PARAMETER SPECIFICATIONS

Table 2: Simulation parameter specification of DAB Bidirectional converter

PARAMETERS	SPECIFICATION
Input Voltage	800 V
Output voltage	500 V
Input current	12.5 A
Output current	20 A
Output Power	10 kW
Phase shift	$-0.44 < \varphi < 0.44$(rad)
Frequency	100 kHz
Turns Ratio	2
Total Leakage Inductance	35 µH

3.1 SIMULATION CIRCUIT

The simulation circuit of the proposed system is shown in figure 6.1. The simulation is done in MATLAB 2022A version with ode45 solver. The continuous power gui is used to run the simulation and visualize the results. The proposed model is simulated in a MATLAB Simulink platform. MATLAB a high-performance language for technical computing integrates computation, visualization and programming in an easy-to-use environment where problems and solutions are expressed in familiar mathematical solution.

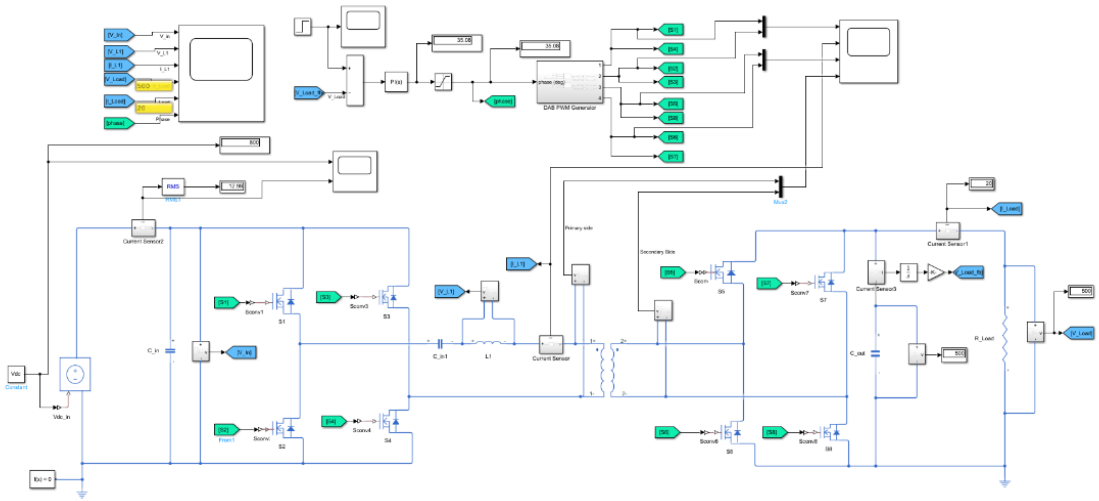

Figure 3.1 Simulation of DAB bidirectional converter.

www.ijprems.com
editor@ijprems.com

INTERNATIONAL JOURNAL OF PROGRESSIVE RESEARCH IN ENGINEERING MANAGEMENT AND SCIENCE (IJPREMS)
(Int Peer Reviewed Journal)
Vol. 04, Issue 12, December 2024, pp : 844-852

e-ISSN : 2583-1062
Impact Factor : 7.001

3.2 SIMULATION RESULT

The system simulation was created utilizing MATLAB/Simulink. A prototype of the DC-DC Converter under consideration has been constructed and examined. In order to attain the target output voltage, the simulation circuit was formulated in MATLAB, incorporating the necessary components available in MATLAB/Simulink.

3.2.1 PWM GENERATOR

The PWM generated is shown in Figure 3.1. A PWM Generator is a circuit or system that produces a Pulse Width Modulated (PWM) signal. PWM signals are square waves with a duty cycle that can be varied to control the power delivered to a load, such as a motor, LED, or other devices.

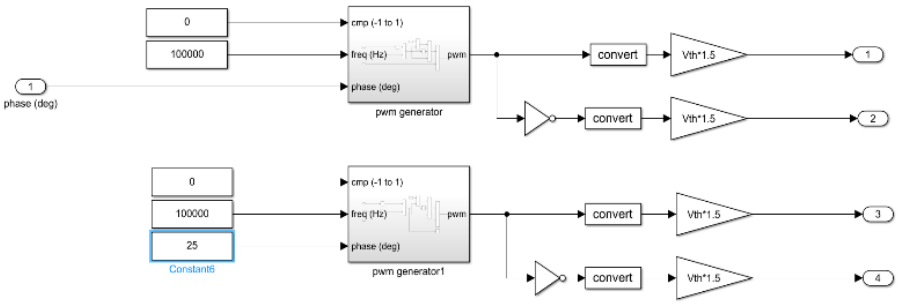

Figure 3.2 PWM generator

3.2.2 SWITCHING PULSES

The switching sequence of the Dual Active Bridge Converter for HB1 to HB2. The PWM signal is generated by using the PWM generator and the signal is controlled by the PI controller control signals. Switching pulses are signals used to control power electronic switches like MOSFETs, IGBTs, and thyristors. These pulses determine when and how the switches turn ON and OFF, enabling the desired operation of power electronic circuits such as inverters, rectifiers, and converters.

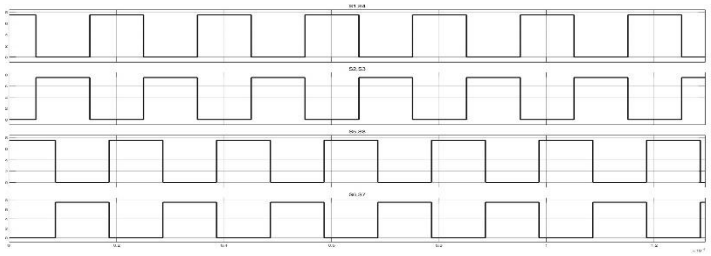

Figure 3.3 Switching pulses of DAB

3.2.3 POWER TRANSFER

In Figures 3.3shows the Power Transfer from HB1 to HB2 These high-frequency square waves are phase shifted with respect to each other. Power transfer takes place from the leading bridge to the lagging bridge, and this power flow direction can be easily changed by reversing the phase shift between the two bridges.

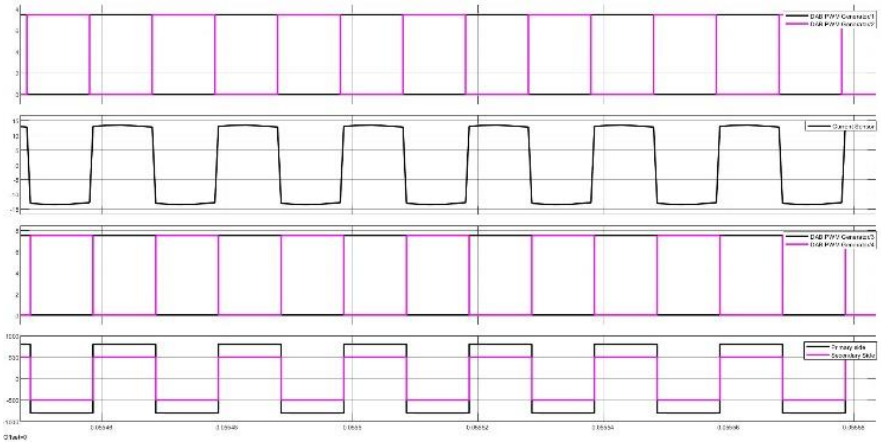

Figure 3.4 Power Transfer from HB1 to HB2

www.ijprems.com
editor@ijprems.com

INTERNATIONAL JOURNAL OF PROGRESSIVE RESEARCH IN ENGINEERING MANAGEMENT AND SCIENCE (IJPREMS)
(Int Peer Reviewed Journal)
Vol. 04, Issue 12, December 2024, pp : 844-852

e-ISSN : 2583-1062
Impact Factor : 7.001

3.2.4 OUTPUT VOLTAGE AND CURRENT

In a bidirectional converter, the output voltage and current are critical parameters that enable energy transfer in both directions between two power sources or storage systems. The converter operates in two modes: boost mode (when energy flows from a lower to a higher voltage level) and buck mode (when energy flows from a higher to a lower voltage level). In boost mode, the output voltage is higher than the input voltage, while in buck mode, it is lower. The output current direction changes based on the energy flow direction, making the converter suitable for applications like battery charging/discharging and renewable energy systems. Effective control strategies, such as current-mode or voltage-mode control, ensure stable output voltage and current regulation during bidirectional operation.

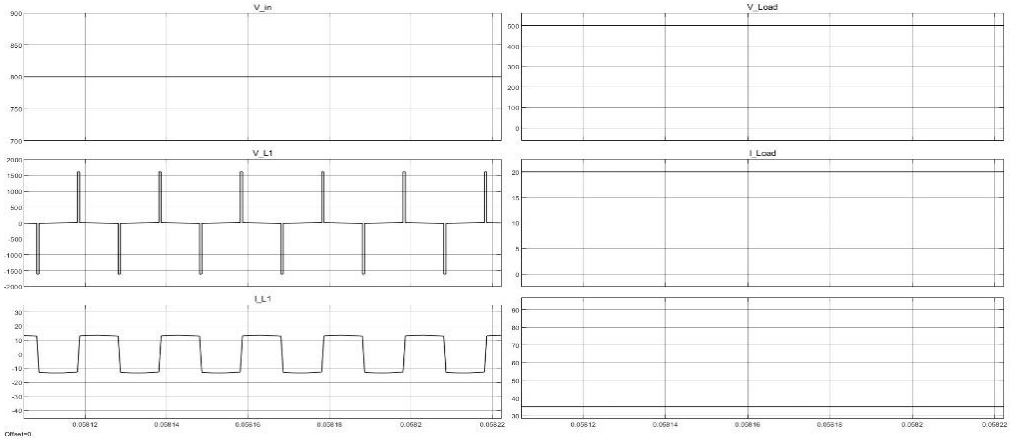

Figure 3.5 Output voltage and Current

4. CONCLUSION

This project successfully demonstrates the design and simulation of a high-gain isolated Dual Active Bridge (DAB) bidirectional DC-DC converter tailored for EV applications. The proposed system integrates advanced power conversion techniques, ensuring efficient and bidirectional power flow—essential for modern EV systems, including regenerative braking and bidirectional battery charging.

The simulation results validate that the designed system achieves high performance in terms of efficiency, stability, and response time, meeting the operational demands of EV powertrains under various load conditions. The optimized design parameters and proposed control strategies highlight the converter's robustness and adaptability for EV power management systems. Thus, the findings confirm that a high-gain isolated DAB converter represents a promising solution for next-generation EV power conversion.

The proposed high-gain isolated DAB bidirectional DC-DC converter offers promising potential for further development and real-world implementation. Future work can focus on experimental validation through hardware implementation to assess practical performance and operational challenges.

Additionally, integrating advanced control strategies such as AI-based adaptive or predictive control could further enhance the system's efficiency, stability, and dynamic response. Exploring multilevel converter architectures could also address higher voltage levels and reduce switching losses, making it suitable for a broader range of EV applications. Further integration with Battery Management Systems (BMS) can optimize state-of-charge management and improve battery life. Moreover, adapting the design for compatibility with renewable energy sources like solar and wind power could enhance the sustainability of EV systems. Lastly, research into scaling this technology for various EV configurations, from two-wheelers to heavy-duty vehicles, could broaden its applicability. These directions will ensure continued innovation and practical feasibility of the proposed converter system for next-generation EV solutions.

5. REFERENCE

[1] E. L. Carvalho, A. Blinov, A. Chub, P. Emiliani, G. de Carne, and D. Vinnikov, ‘‘Grid integration of DC buildings: Standards, requirements and power converter topologies,’’ IEEE Open J. Power Electron., vol.3, pp. 798–823, 2022.

[2] E. L. Carvalho, L. V. Bellinaso, R. Cardoso, and L. Michels, ‘‘Distributed price-based power management for multibuses DC nanogrids EEMS,’’ IEEE J. Emerg. Sel. Topics Power Electron., vol. 10, no. 5, pp. 5509–5521, Oct. 2022.

[3] M. Veerachary, “General Rules for Signal Flow Graph Modeling and Analysis of DC-DC Converters”, IEEE Trans. On Aerospace and Electronics Systems, Vol. 40, No. 1, pp. 259-271, Jan, 2020.

[4] A. Blinov, R. Kosenko, D. Vinnikov, and L. Parsa, ''Bidirectional isolated current-source DAB converter with extended ZVS/ZCS range and reduced energy circulation for storage applications,'' IEEE Trans. Ind. Electron., vol. 67, no. 12, pp. 10552–10563, Dec. 2020.

[5] X. Pan, H. Li, Y. Liu, T. Zhao, C. Ju, and A. K. Rathore, ''An overview and comprehensive comparative evaluation of current-fedisolated- bidirectional DC/DC converter,'' IEEE Trans. Power Electron., vol. 35, no. 3, pp. 2737–2763, Mar. 2020.

[6] S. Shao, H. Chen, X. Wu, J. Zhang, and K. Sheng, ''Circulating current and ZVS-on of a dual active bridge DC–DC converter: A review,'' IEEE Access, vol. 7, pp. 50561–50572, 2019.

[7] J. Sha, L. Chen, and G. Zhou, ''Discrete extended-phase-shift control for dual-active-bridge DC–DC converter with fast dynamic response,'' IEEE Trans. Ind. Electron., vol. 70, no. 6, pp. 5662–5673, Jun. 2023.

[8] W. Zhao, X. Zhang, S. Gao, and M. Ma, ''Improved model-based phaseshift control for fast dynamic response of dual-active-bridge DC/DC converters,'' IEEE J. Emerg. Sel. Topics Power Electron., vol. 9, no. 1, pp. 223–231, Feb. 2021.

[9] F. Lin, X. Zhang, X. Li, C. Sun, W. Cai, and Z. Zhang, ''Automatic triple phase-shift modulation for DAB converter with minimized power loss,'' IEEE Trans. Ind. Appl., vol. 58, no. 3, pp. 3840–3851, May 2022.

[10] D. Sha, J. Zhang, and K. Liu, ''Leakage inductor current peak optimization for dual-transformer current-fed dual active bridge DC–DC converter with wide input and output voltage range,'' IEEE Trans. Power Electron., vol. 35, no. 6, pp. 6012–6024, Jun. 2020

[11] M. Mahdavifard, N. Mazloum, F. Zahin, A. KhakparvarYazdi, A. Abasian, and S. A. Khajehoddin, ''An asymmetrical DAB converter modulation and control systems to extend the ZVS range and improve efficiency,'' IEEE Trans. Power Electron., vol. 37, no. 10, pp. 12774–12792, Oct. 2022.

[12] G. Thiele and E. Bayer, Voltage Doubler/Tripler Current-Mode Charge Pump Topology with Simple "Gear Box", 38th IEEE Powern Electronics Specialists Conference, 2021

[13] Texas Instruments. (2011). Phase-Shifted Full-Bridge, Zero-Voltage Transition Design Considerations. [Online]. Available: http://www. ti.com/lit/an/slua107a/slua107a.pdf

[14] J. Deng and H.Wang, ''Ahybrid-bridge and hybrid modulation-based dual active-bridge converter adapted to wide voltage range,'' IEEE J. Emerg. Sel. Topics Power Electron., vol. 9, no. 1, pp. 910–920, Feb. 2021.

[15] Y.Yan, H. Gui, and H. Bai, ''Complete ZVS analysis in dual active bridge,'' IEEE Trans. Power Electron., vol. 36, no. 2, pp. 1247–1252, Feb. 2021.

[16] Y. Tang, W. Hu, D. Cao, N. Hou, Z. Li, Y. W. Li, Z. Chen, and F. Blaabjerg, ''Deep reinforcement learning aided variable-frequency triple-phase-shift control for dual-active-bridge converter,'' IEEE Trans. Ind. Electron., vol. 70, no. 10, pp. 10506–10515, Oct. 2023.

[17] M. Capó-Lliteras, G. G. Oggier, E. Bullich-Massagué, D. Heredero-Peris, and D. Montesinos-Miracle, ''Analytical and normalized equations to implement the optimized triple phase-shift modulation strategy for DAB converters,'' IEEE J. Emerg. Sel. Topics Power Electron., vol. 11, no. 3, pp. 3535–3546, Jun. 2023.

[18] H. Xie, F. Cai, J. Jiang, and D. Li, ''A fundamental harmonic analysis based optimized scheme for DAB converters with lower RMS current and wider ZVS range,'' IEEE Trans. Transport. Electrific., vol. 9, no. 3, pp. 4045–4058, Sep. 2023.

[19] A. Kazemtarghi, S. Dey, A. Mallik, and N. G. Johnson, ''Asymmetric half frequency modulation in DAB to optimize the conduction and switching losses in EV charging applications,'' IEEE Trans. Transport. Electrific., vol. 9, no. 3, pp. 4196–4210, Sep. 2023.

[20] D. Mou, Q. Luo, J. Li, Y.Wei, Z.Wang, P. Sun, X. Du, and H. A. Mantooth, ''Hybrid duty modulation for dual active bridge converter to minimize RMS current and extend soft-switching range using the frequency domain analysis,'' IEEE Trans. Power Electron., vol. 36, no. 4, pp. 4738–4751, Apr. 2021.